Observation of double-charge discrete vortex solitons in hexagonal photonic lattices

Bernd Terhalle,[1,2] Tobias Richter,[3] Kody J. H. Law,[4] Dennis Göries,[2] Patrick Rose,[2] Tristram J. Alexander,[1] Panayotis G. Kevrekidis,[4] Anton S. Desyatnikov,[1] Wieslaw Krolikowski,[1] Friedemann Kaiser,[3] Cornelia Denz,[2] and Yuri S. Kivshar[1]

[1]*Nonlinear Physics Center and Laser Physics Center, Research School of Physics and Engineering, The Australian National University, Canberra ACT 0200, Australia*

[2]*Institut für Angewandte Physik and Center for Nonlinear Science (CeNoS), Westfälische Wilhelms-Universität, 48149 Münster, Germany*

[3]*Institut für Angewandte Physik, Technische Universität Darmstadt, Darmstadt, Germany*

[4]*Department of Mathematics and Statistics, University of Massachusetts, Amherst, Massachusetts 01003-4515, USA*

(Received 5 February 2009; published 21 April 2009)

We report on the experimental observation of stable double-charge discrete vortex solitons generated in hexagonal photonic lattices created optically in self-focusing nonlinear media and show that single-charge vortex solitons are unstable in analogous conditions. Subsequently, we study, both theoretically and experimentally, the existence and stability of spatial vortex solitons in two-dimensional hexagonal photonic lattices. We demonstrate that the stability of the double-charge vortices is a consequence of the intersite power exchange in the vortex soliton, and we provide a simple stability criterion on the basis of the analysis of the corresponding discrete nonlinear model. We extend our analysis to the case of defocusing nonlinearity and show the inversion of the vortex stability properties resulting in the fact that single-charge vortices become stable while their double-charge counterparts are unstable.

DOI: 10.1103/PhysRevA.79.043821 PACS number(s): 42.65.Tg

I. INTRODUCTION

Experiments with optical vortices have proven to be some of the most spectacular in the study of nonlinear light propagation in periodic photonic structures due to often unexpected properties of the vortex flows [1]. Previous works studied the vortices in square photonic lattices, and they revealed that when a self-trapped vortex beam is placed on a discrete structure of the lattice, it retains a phase singularity with a particular winding number (or charge) [2–4]. These early experiments on the generation of single-charge discrete vortices were quickly followed by the demonstration of the complex dynamics of single-charge vortex states such as transmutations between different spatial profiles [5] and even the inversion of the vortex charge [6,7]. More recently, the lattices of nonsquare symmetry have been considered, such as hexagonal and honeycomb lattices [8–11], with striking new vortex forms found, including the multivortex localized states [12,13]. However, perhaps the most counterintuitive result to emerge from the consideration of hexagonal lattices is that in the simplest six-site configuration double-charge vortices may become stable, while single-charge vortices are always unstable [14], in agreement with the stability properties of vortex solitons in modulated Bessel lattices [15]. This is particularly surprising as higher-charge discrete vortices are typically unstable in homogeneous nonlinear systems [1].

The main objective of this work is to demonstrate experimentally, numerically, and theoretically the stability of a double-charge vortex in contrast to the corresponding single-charge vortex state which is unstable under the same conditions. We extend the earlier theoretical work for isotropic systems and study the full anisotropic model of nonlinear media with the numerical results supporting our experimental observations. To provide an additional theoretical insight on this stabilization effect, we employ a simpler discrete model to examine the effect of the lattice stretching on the vortex stability, and also showcase the inversion of the vortex stability picture (between single- and double-charge vortices) in the case of the defocusing nonlinear response.

The outline of the paper is the following. In Sec. II we introduce our experimental setup and present the results of the experimental observation of stable double-charge vortices in a hexagonal photonic lattice created in a crystal with photorefractive nonlinearity in the self-focusing regime. We also show that in this regime single-charge vortices are unstable. In Sec. III we extend the theoretical results of Ref. [14] and analyze numerically the full anisotropic model of photorefractive nonlinearity demonstrating a good agreement between the numerical and experimental results. In Sec. IV we use a discrete model to examine theoretically the effect of the lattice stretching on the stability of the double-charge vortex and determine a critical stretching parameter for the vortex stabilization. Section V describes the experimental observation of stable single-charge vortices and unstable double-charge vortices in the defocusing nonlinear regime, confirming the inversion of the vortex stability established theoretically on the basis of a discrete model. Finally, Sec. VI concludes the paper.

II. EXPERIMENTAL RESULTS

First, we demonstrate experimentally the stable generation of a double-charge vortex in a photorefractive crystal in the presence of a hexagonal photonic lattice in the self-focusing regime, as predicted theoretically for an isotropic model [14]. The experimental setup is shown schematically in Fig. 1, and it is similar to that used earlier in Ref. [16]. A beam from a frequency-doubled Nd:YAG laser at a wavelength of 532 nm is split into two beams with a beam splitter,

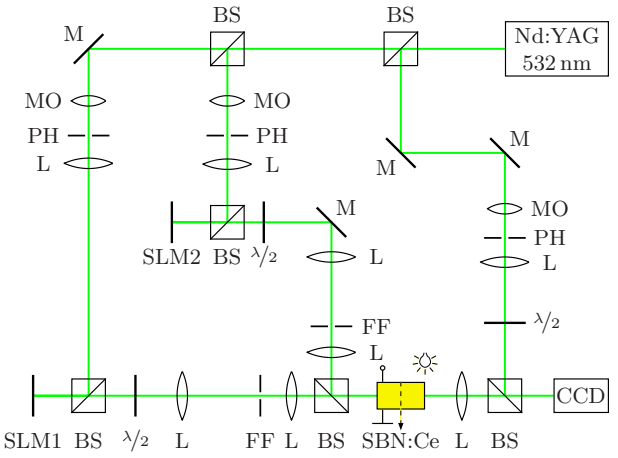

FIG. 1. (Color online) Schematic of the experimental setup. BS: beam splitter; CCD: camera; FF: Fourier filter; L: lens; M: mirror; MO: microscope objective; PH: pinhole; SLM: spatial light modulator.

and the separate beams are used to illuminate two programmable spatial light modulators.

The first spatial light modulator (SLM1, see Fig. 1) converts the incoming beam into three interfering plane waves which are imaged onto the front face of a 20 mm long photorefractive $Sr_{0.60}Ba_{0.40}Nb_2O_6$ (SBN:Ce) crystal which is externally biased with a dc electric field directed along its optical c axis. The resulting interference pattern is that of a two-dimensional hexagonal photonic lattice (Fig. 2) with a lattice power of $I_{\mathrm{latt}} \approx 75$ μW. A half-wave plate ensures the polarization of the lattice beam to be ordinary, so during the beam propagation through the crystal the nonlinear effects are negligible [17]. The lattice is oriented such that the light intensity maxima of the hexagonal pattern are aligned along the lines parallel to the optical axis of the crystal in the so-called "horizontal configuration." The periodic light intensity distribution induces a corresponding refractive index pattern via the photorefractive effect [17] forming the optical lattice. Due to the anisotropic nature of the nonlinear response of the crystal this optically induced refractive index does not preserve the symmetry of the lattice beam. In particular, the modulation of the refractive index is stronger along the optical axis than along the diagonals, making the resulting optical coupling between refractive index maxima very asymmetric (see Fig. 2, top row). To counteract the effect of the anisotropy, the lattice forming beams are tilted to induce a stretching of the lattice along the vertical direction such that the optical coupling between lattice maxima is closer to that of the original hexagonal symmetry of the lattice [13], yielding lattice constants of $d_y = 62$ μm and $d_x = 27$ μm for the vertical and horizontal directions, respectively. This gives a ratio of $d_y/d_x \approx 2.2$ as opposed to the ratio $d_y/d_x = \sqrt{3}$ of a symmetric lattice. The importance of the lattice stretching for the vortex stability is examined theoretically below in Sec. IV.

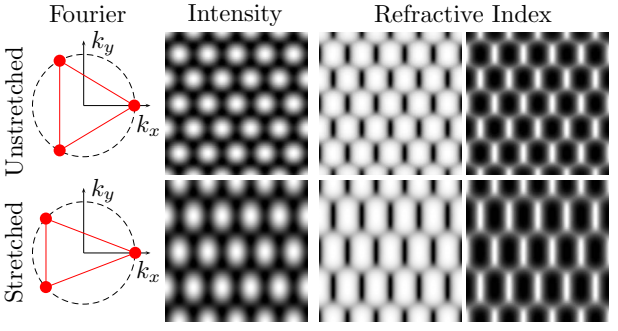

FIG. 2. (Color online) Sketch of the Fourier image and numerically calculated lattice intensity and refractive index profiles for the symmetric hexagonal lattice (top panels) and the stretched lattice (bottom panels). The lattice beams in Fourier space are indicated by dots forming an equilateral triangle for the unstretched lattice and an isosceles triangle for the stretched lattice. The refractive index profiles are shown for focusing (left) and defocusing (right) nonlinearities.

The second spatial light modulator (SLM2, see Fig. 1) combined with proper Fourier filtering [18,19] is employed to achieve the desired amplitude and phase structure of an incident Gaussian probe beam. The polarization of the probe beam is extraordinary so it propagates through the crystal in the nonlinear regime. The strength of nonlinearity is controlled by varying an applied external dc electric field. In all our experiments the value of the bias potential was set to be approximately 2.2 kV/cm. In order to visualize the phase structure of the probe beam, a third beam is derived from the laser. It is passed through a half-wave plate to ensure its extraordinary polarization and subsequently sent directly to the charge-coupled device (CCD) camera to record a phase interferogram with the probe beam.

We use the phase modulator to impose either a 2π or 4π phase winding on an input modulated (six-site) beam for the generation of single- and double-charge vortices, respectively. The characteristics of the beams are otherwise identical, and thus any differences in the dynamics are due solely to the different input phases. We selectively vary the input beam intensity to effectively move from the linear regime (low power, $I_{\mathrm{probe}} \approx 50$ nW) to the nonlinear regime (high power, $I_{\mathrm{probe}} \approx 550$ nW).

The single-charge vortex input is shown in Fig. 3(a). Its intensity distribution has a form of a necklace with six intensity peaks whose positions correspond to the lattice sites (index maxima). At low input power the beam undergoes discrete diffraction and a complete loss of the initial six-site input state [Fig. 3(b)]. At high power the initial six-site intensity profile changes significantly after propagation [Fig. 3(c)], showing strong intensity modulations and even filling in the central lattice site. Furthermore, in the phase profile multiple vortices are seen to appear, further indicating a breakdown of the single-charge state [circles in bottom panel of Fig. 3(c)]. We were unable to find an example of stable propagation of the single-charge vortex in the high-power (nonlinear) regime, a result consistent with the isotropic case predictions of Ref [14]. (see also the analysis below for the anisotropic case).

In the case of the double-charge vortex input [see Fig. 4(a)] we again observe a discrete diffraction with low input power [see Fig. 4(b)]; however the result changes dramatically when the power is increased [see Fig. 4(c)]. We observe that now the six-site input structure is preserved in the non-

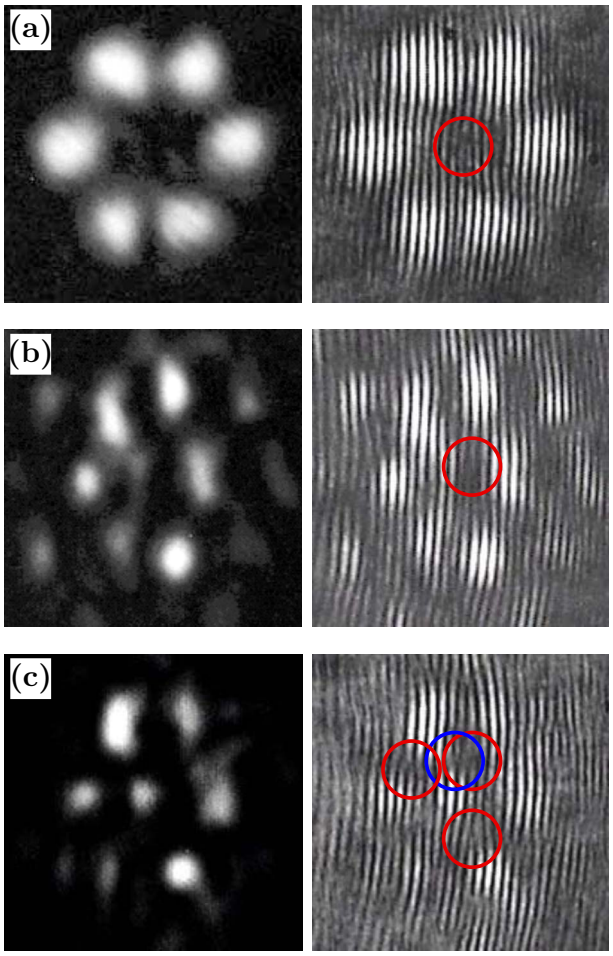

FIG. 3. (Color online) (a) An input single-charge vortex beam; (b) the beam profile and phase at the output crystal face for low input intensity; (c) output for high input intensity. In both cases we see the breakup of the single-charge vortex. Here and below in experimental figures: left panels show intensity; right panels reveal phase structure; circles indicate positions of vortices with charge $m=+1$ (red) and $m=-1$ (blue).

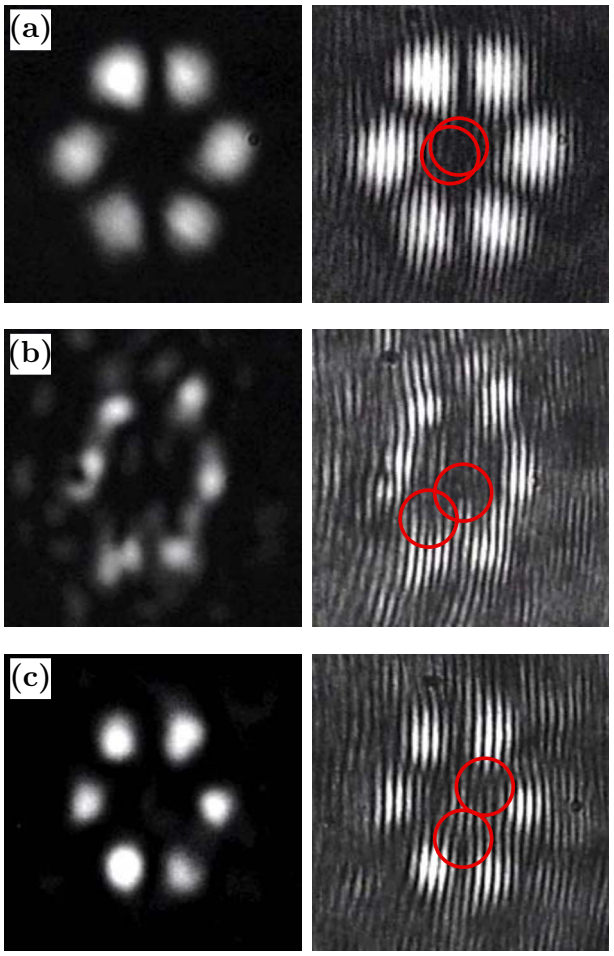

FIG. 4. (Color online) The same as in Fig. 3, but for the case when the input beam (a) has a double-charge vortex phase. (b) Output at the crystal face demonstrates discrete diffraction for low power and (c) discrete double-charge vortex generation at high power.

linear propagation. Interestingly, while the overall phase winding is still 4π, it is seen that the initial double-charge singularity has split into two single-charge vortices [circles in the lower panel of Fig. 4(c)]. This splitting of the higher-order singularity can be attributed to an inherent topological instability in the higher phase winding [20]. This topological breakdown in the linear (low power) part of the field further indicates that the stability of the 4π phase winding across the six sites is due to the interplay of the nonlinearity and local phase of the high-power sites suppressing the development of a dynamical instability [14]. However, we find that this stability is critically dependent on the symmetry of the lattice, with a decrease in the lattice stretching (and thus a corresponding decrease in the symmetry of the underlying modulated refractive index), leading to a dynamical instability in the double-charge state as well. The phase interferogram in Fig. 4(c) also indicates an additional pair of single-charge vortices of the opposite charge inside the vortex structure (not marked by circles). However, this additional pair does not affect the stability of the 4π phase winding, and it can be fully attributed to inevitable experimental noise in this region of low intensity of light.

III. NUMERICAL SIMULATIONS

In the earlier work examining double-charge vortex stability the isotropic nonlinear model was used [14], which does not take into account anisotropy of the photorefractive nonlinearity and the stretching of the lattice. Therefore, to corroborate our experimental results, here we use the full anisotropic model. The propagation of a scalar probe field A through a photorefractive crystal is given by

$$2i\frac{\partial A}{\partial z}+\nabla_{\perp}^{2}A-\gamma_{\mathrm{nl}}E_{\mathrm{sc}}(I_{\mathrm{tot}})A=0, \tag{1}$$

where $\nabla_{\perp}^{2}=\partial^{2}/\partial x^{2}+\partial^{2}/\partial y^{2}$; $I_{\mathrm{tot}}=|A_{\mathrm{latt}}|^{2}+|A|^{2}$, A_{latt} is the periodic lattice wave, and $\gamma_{\mathrm{nl}}=k_{0}^{2}w_{0}^{2}n_{0}^{4}r_{\mathrm{eff}}$ is the photorefractive nonlinearity coefficient proportional to the effective element r_{eff} of the linear electro-optic tensor. Spatially localized and stationary solutions of Eq. (1) can be found in the form $A(x,y,z)=a(x,y)\exp(i\beta z)$, where β is the soliton propaga-

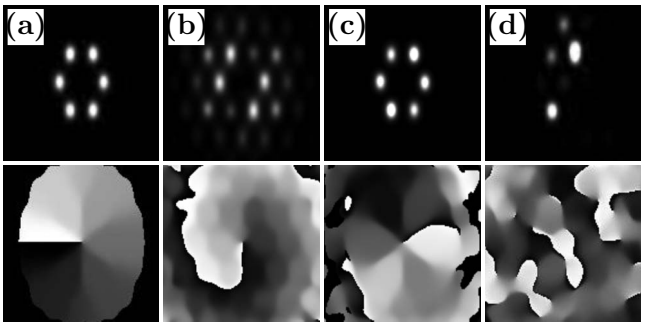

FIG. 5. Numerical simulation of a single-charge vortex (E_{ext} =2.5 kV/cm, $I_{latt}=|A_{latt}|^2=1$, $\beta=3$). (a) Initial vortex beam profile; (b) beam profile at $z=20$ mm for low input power; (c) beam profile at $z=20$ mm for high input power; (d) high-power output at $z=280$ mm. Top panels: intensity; bottom panels: phase.

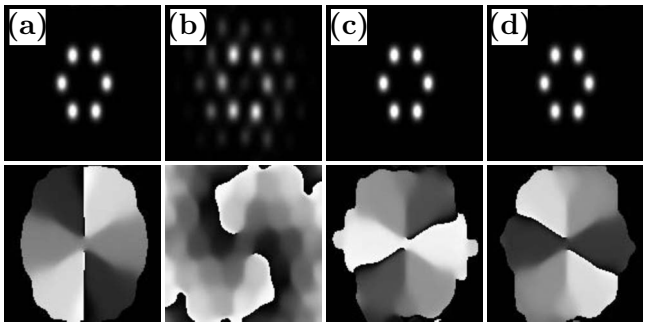

FIG. 6. Numerical simulation of a double-charge vortex (E_{ext} =2.5 kV/cm, $I_{latt}=|A_{latt}|^2=1$, $\beta=3$). (a) Initial vortex beam profile; (b) beam profile at $z=20$ mm for low input power; (c) beam profile at $z=20$ mm for high input power; (d) high-power output at $z=280$ mm. Top panels: intensity; bottom panels: phase.

tion constant. The electric screening field E_{sc} is generated by the separation of optically excited charges which drift in the external electric field. This directional drift is responsible for an anisotropy of the total electric field in the crystal and consequently an anisotropic refractive index change. A quantitative model describing the stationary dynamics has been proposed in terms of the scalar potential ϕ from which the screening field may be found through $E_{sc}=-\partial_x\phi$. The equation describing the evolution of this potential is given by [21]

$$\nabla_\perp^2\phi+\nabla_\perp\ln(1+I_{tot})\nabla_\perp\phi=E_{ext}\partial_x\ln(1+I_{tot}), \qquad (2)$$

where E_{ext} is the dc bias voltage applied along the optical axis of the crystal which is taken to be the x axis. The transverse coordinates (x,y) and propagation coordinate z are measured in units of the characteristic lengths w_0 and z_0, respectively, where $z_0=k_z w_0^2$ and $k_z=n_0k_0$ with $k_0=2\pi/\lambda$. In particular, we use a transverse scale of $w_0=10$ μm and λ and n_0 as for the experiment. The total intensity I_{tot} is normalized in units of the background illumination and we take $E_{ext}=2.5$ kV/cm. For the lattice wave we use the expression

$$A_{latt}=\exp(2ik_x x/3)+\exp(-ik_x x/3+ik_y y)+\exp(-ik_x x/3-ik_y y), \qquad (3)$$

leading to a diffraction-free hexagonal pattern with the horizontal orientational symmetry shown in Fig. 2. We consider a stretched lattice with $k_x/k_y=2.5$ and spatial separations of lattice maxima of $d_x=2\pi/k_x=2$ in x and $d_y=2\pi/k_y=5$ in y directions (lattice spacings of 20 and 50 mm, respectively).

First we consider the case of a six-site initial state with a single-charge vortex phase of the form shown in Fig. 5(a) with either low or high power propagating a distance of z =20 mm in the lattice. For the low input power case [Fig. 5(b)] we see that, as in the experiment, the vortex beam undergoes strong diffraction and break-up. If instead a high input power is considered [Fig. 5(c)] the vortex maintains much of its form. Some intensity fluctuations are evident, and more importantly, the vortex phase has deteriorated showing breakdown of the initial single-charge vortex circulation. It must be noted that the breakup is clearly less than that observed in the experiment and this discrepancy is attributed to the higher anisotropy of the experimental lattice leading to a larger instability growth rate. In our numerical simulations, the strong instability becomes evident for longer propagation distances as shown in Fig. 5(d) for $z=280$ mm.

In Fig. 6 we consider the same input beam intensities but change the phase to that of a double-charge vortex, as shown in Fig. 6(a). The low power output in Fig. 6(b) appears similar to the single-charge case, exhibiting diffraction and breakup of the vortex. In contrast, the high-power output in Figs. 6(c) and 6(d) appears unchanged in the intensity profile with a well-pronounced double-charge vortex phase. Similar to the experimental results, the separation of the double-charge phase singularity into two single-charge singularities is observed, including in the initial condition in Fig. 6(a). However the phase circulation around a contour tracing the six high intensity sites is well defined and equals 4π.

IV. EFFECT OF LATTICE STRETCHING

A key feature of the full model considered here, as compared to the isotropic case studied earlier [14], is the presence of anisotropy. In the experiment and in numerical simulations, we have sought to reduce the effects of the anisotropy by stretching the lattice. In this section we use a discrete model to obtain some further insight, based on semi-analytical considerations, on how the lattice stretching (or more generally the symmetries of the intersite coupling) affects the discrete vortex stability.

Within the framework of the discrete approximation the hexagonal lattice corresponds to a coupled waveguide array with complex amplitudes $u_{m,n}$ of the electric field governed by the following system:

$$i\frac{du_{m,n}}{dz}=-\varepsilon\sum_{m',n'}C_{m',n'}u_{m',n'}+(4+2C)\varepsilon u_{m,n}-b|u_{m,n}|^2u_{m,n}, \qquad (4)$$

where the constant ε denotes the strength of linear coupling between waveguides, $b=1$ is for self-focusing, and $b=-1$ is for self-defocusing media. The set $\{m',n'\}$ indexes the six nearest neighboring sites to the site (m,n), a pair in each of the three principal directions. The parameters $C_{m',n'}$ account

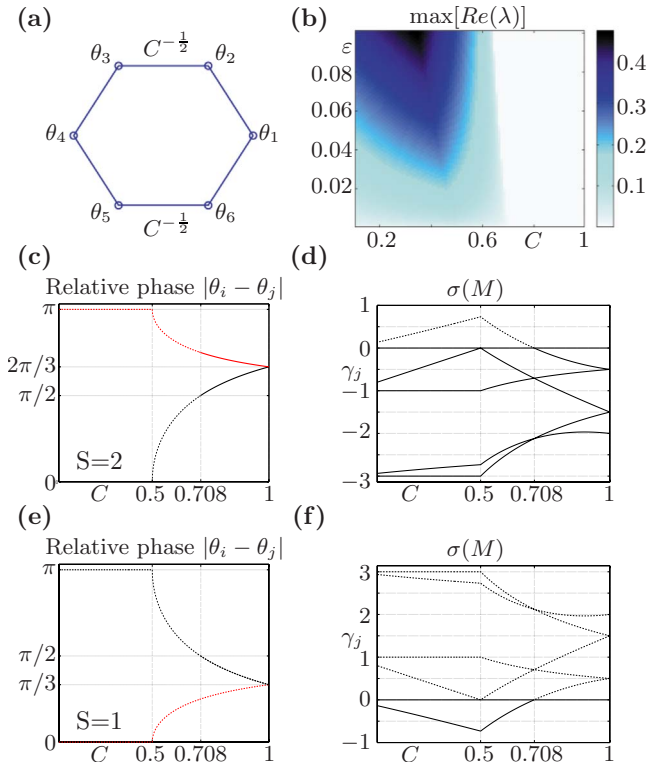

FIG. 7. (Color online) The hexagonal cell is approximated by a contour shown in (a). The images below this show the relative phases for the (c) double- and (e) single-charge vortices distinguishing stable (with $\gamma_j<0$ for all j) and unstable (with $\gamma_j>0$) solutions. For $C=1$ the phases of adjacent excited nodes are equidistant and all are a distance of $2\pi/3$ or $\pi/3$ from one another. These are the isotropic double- and single-charge vortices. For smaller C, the relative phase of θ_2 and θ_3 (shown in black) becomes smaller for the double-charge (c) solution [and larger for the single charge (e)] and when $|\theta_2-\theta_3|<(>)\pi/2$, for $C<C_{\rm cr}=0.708$, one corresponding eigendirection becomes unstable (stable). This can be observed in (d) and (f), in which the six eigenvalues of the linearization matrix $\mathcal{M}$ are presented as a function of C. When they are all negative the solution is stable close to the anticontinuum limit. Notice for the $S=2$ solution (d) the smallest magnitude one becomes positive for $C<C_{\rm cr}$, leading to instability. (b) The bifurcation of the relevant eigenvalue of the $S=2$ vortex through the origin is represented by the maximum real part of the linearization spectrum, max[Re (λ)] as a function of both the anisotropy parameter, C, as well as the coupling ε. Notice the critical point (in C) shifts only very slightly from the first-order prediction for $0<\varepsilon<0.1$.

for the coupling anisotropy and are equal to C for the neighbors lying along the (1,0) direction and 1 otherwise.

In the anticontinuum limit $\varepsilon\to 0$, i.e., for very weak interaction between neighboring waveguides, the solutions of Eq. (4) can easily be found in the general form $u_{m,n}=\sqrt{\beta}\exp\{-i\beta z+i\theta_{m,n}\}$ for arbitrary $\theta_{m,n}\in[0,2\pi)$ [22]. Letting $\beta=1$ without loss of generality and using j to index the sites along the six-site one-dimensional contour shown in Fig. 7(a), the condition for existence of solutions with $\varepsilon>0$ reduces to the vanishing of the total power flow at each site,

$$c_{j,j-1}\sin(\theta_j-\theta_{j-1})+c_{j,j+1}\sin(\theta_j-\theta_{j+1})=0, \tag{5}$$

subject to periodic boundary conditions $\theta_{j+6}=\theta_j$ for $j=1,\ldots,6$ [22]. Similar to $C_{m',n'}$ above the constants $c_{j,k}$ account for the coupling anisotropy,

$$c_{j,k}=\begin{cases} C, & (j,k)\in\{(2,3),(3,2),(5,6),(6,5)\} \\ 1, & \text{otherwise}. \end{cases} \tag{6}$$

We consider first the focusing medium with $b=1$. In the case $C=1$, the single- and double-charge vortex solitons exist close to the anticontinuum limit as defined by the phase vectors $\theta_j=Sj\pi/3$, where $S=1,2$, respectively. An analytical approximation for the stability of the discrete solitons can be made for small ε based on an appropriate modification of the theory originally developed in Ref. [22] for the isotropic square lattice. The stability can be determined from the eigenvalues γ_j of the 6×6 Jacobian of Eq. (5),

$$(\mathcal{M})_{j,k}=\begin{cases} b[c_{j,j+1}\cos(\theta_{j+1}-\theta_j)+c_{j,j-1}\cos(\theta_{j-1}-\theta_j)], & j=k \\ -b[c_{j,k}\cos(\theta_j-\theta_k)], & j=k\pm 1 \\ 0, & |k-j|\geq 2. \end{cases} \tag{7}$$

For each eigenvalue γ_j, the full linearization around a stationary solution will have eigenvalue pairs λ_j given, to leading order, by $\lambda_j=\pm\sqrt{2\gamma_j\varepsilon}$. Therefore, the sign of the eigenvalues of $\mathcal{M}$ determines whether the eigenvalues of the bifurcating solution will be real or imaginary. In particular, positive eigenvalues of $\mathcal{M}$ will indicate real eigenvalues of the full linearization problem, and, hence, instability for this Hamiltonian system.

The results for the existence and stability of single- and double-charge vortex configurations are presented in Figs. 7(c)–7(f) for $C\in[0.1,1]$. The results for $1<C<10$ are not shown since no new instabilities arise in that regime. These results can be summarized as follows:

(i) The $S=2$ vortex is stable for $C>C_{\rm cr}=0.708$, as it is in the isotropic case [14].

(ii) As two of the relative phase pairs decrease below $\pi/2$ due to the stretching, the $S=2$ vortex becomes destabilized for $C<C_{\rm cr}=0.708$ due to an effective modulational instability [14] (see also Ref. [23] for a general analysis of the instability) along the one-dimensional six-site contour.

(iii) Below a stretching of $C=0.5$, the $S=2$ configuration becomes real with $\theta_1=\theta_4=0$ and the others equal to π, (or vice versa).

(iv) On the other hand, the vortex with $S=1$ is unstable throughout the considered interval of stretching parameter, but also degenerates into a real solution with $\theta_{3,4,5}=0$ and the others equal to π.

A continuation of solutions for the double-charge family was performed in the coupling parameter ε, and the critical value $C_{\rm cr}$, represented by the front of real eigenvalues, was found to deviate very weakly from the first order prediction, when ε was varied in the interval [0,0.1]. The stability results are detailed in Figs. 7(b) and 7(d).

We can use full anisotropic models (1) and (2) to estimate the relative coupling values typically used in experiments. In the unstretched case we calculate the anisotropy parameter to be $C \approx 0.22$, while with the lattice stretching this becomes $C \approx 0.82$. These values have been calculated for the particular case of the high input beam intensity although they depend strongly on both the lattice depth and the beam intensity. It is evident however that the unstretched value places the lattice in a regime where no stable vortex formation is expected from the discrete model analysis, in agreement with experiment. Furthermore, in the stretched case we can see that again in accordance with the analysis of the discrete model a stretching parameter of $C=0.82$ is within the stable region of double-charge vortex formation, as was also confirmed experimentally. We thus illustrate a very good agreement between the predictions of the discrete model, the parameters calculated from the full anisotropic model, and the actual experimental results.

One of the advantages of the discrete model is that the relevant theoretical analysis can be straightforwardly extended to the case of the defocusing nonlinearity. In particular, it is well known that a so-called *staggering transformation* along the contour of such a solution for a given b, i.e., $\tilde{U}_j=(-1)^j U_j$, yields a solution to the problem with $\tilde{b}=-b$; this illustrates that a mere staggering transformation suffices to extend the focusing results above to the defocusing case. More specifically, the staggering transformation of the $S=1$ focusing solution leads to the $S=-2$ (or equivalently $S=2$) solution for the defocusing case, while that of the $S=2$ focusing vortex leads to the $S=-1$ (or equivalently $S=1$) defocusing vortex. Importantly also, the stability results for single- and double-charge solutions for the focusing case immediately translate to their defocusing counterparts, namely, the double- and single-charge solutions (respectively). Since the stability predictions are exactly reversed in the defocusing case (between the single- and double-charged vortex), numerical and experimental studies have also been performed in this setting to test the theoretical prediction.

V. DEFOCUSING NONLINEARITY

As discussed above, the stability properties of single- and double-charge vortices with focusing nonlinearity are expected to be inverted when the nonlinearity is changed from focusing to defocusing. For completeness of our analysis, we examine this situation numerically as well as experimentally and confirm this general theoretical prediction.

Similar to the focusing case, we perform numerical simulations using full anisotropic models (1) and (2) but reverse the sign of the nonlinearity by using $E_{\text{ext}}=-2.5$ kV/cm.

Figure 8 summarizes the results for the single-charge vortex and it clearly demonstrates the inverted stability properties caused by the defocusing nonlinearity. In contrast to the focusing case (Fig. 5), intensity and phase profiles of the input structure are preserved and a stable single-charge discrete vortex soliton is formed. It should be noted, however, that in the low intensity regime (Fig. 8) the diffraction is much less pronounced than in the presence of a focusing nonlinearity and hardly visible for propagation distances of

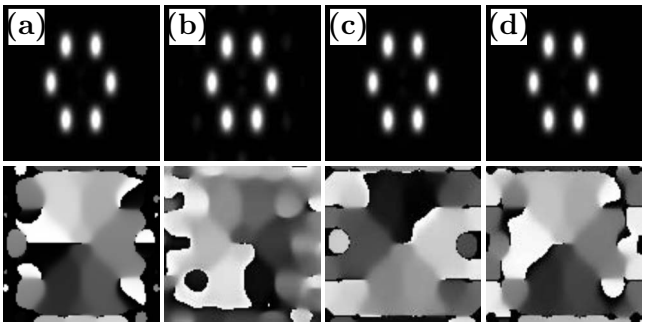

FIG. 8. Numerical simulation of a single-charge vortex for defocusing nonlinearity ($E_{\text{ext}}=-2.5$ kV/cm, $I_{\text{latt}}=|A_{\text{latt}}|^2=4$, $\beta=2$). (a) Initial vortex beam profile; (b) beam profile at $z=20$ mm for low input power; (c) beam profile at $z=20$ mm for high input power; (d) high-power output at $z=280$ mm. Top panels: intensity; bottom panels: phase.

20 mm (Fig. 8). The same result is obtained for the low-intensity double-charge vortex shown in Fig. 9(b). Moreover, compared to the focusing case, the instability is weaker and more evident in the phase than in the intensity [Figs. 9(c) and 9(d)]. Overall, however, the numerical simulations well confirm the theoretical prediction of inverted stability properties in the defocusing case, resulting in a stable single-charge vortex soliton and an unstable double-charge vortex.

Experimentally, the nonlinearity can also be made defocusing by simply inverting the external bias voltage. We consider a bias field of ~ 1.6 kV/cm antiparallel to the optical axis. Our photonic lattice beam is 50 μW; we produce a stretched lattice with the same lattice constants as in the self-focusing case. Notice that now the lattice acquires a honeycomb structure, i.e., light intensity maxima of the lattice forming beams lead to minima of the corresponding refractive index pattern (see bottom panels in Fig. 2). It is important to note here that as the theoretical stability results of the discrete model are obtained from the consideration of the one-dimensional six-site contour with periodic boundary conditions, these results are unaffected by the honeycomb structure of the defocusing photorefractive crystal lattice. For each vortex input we consider two different input beam pow-

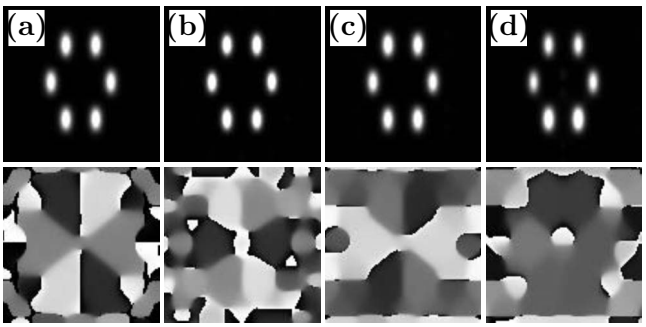

FIG. 9. Numerical simulation of a double-charge vortex for defocusing nonlinearity ($E_{\text{ext}}=-2.5$ kV/cm, $I_{\text{latt}}=|A_{\text{latt}}|^2=4$, $\beta=2$). (a) Initial vortex beam profile; (b) beam profile at $z=20$ mm for low input power; (c) beam profile at $z=20$ mm for high input power; (d) high-power output at $z=280$ mm. Top panels: intensity; bottom panels: phase.

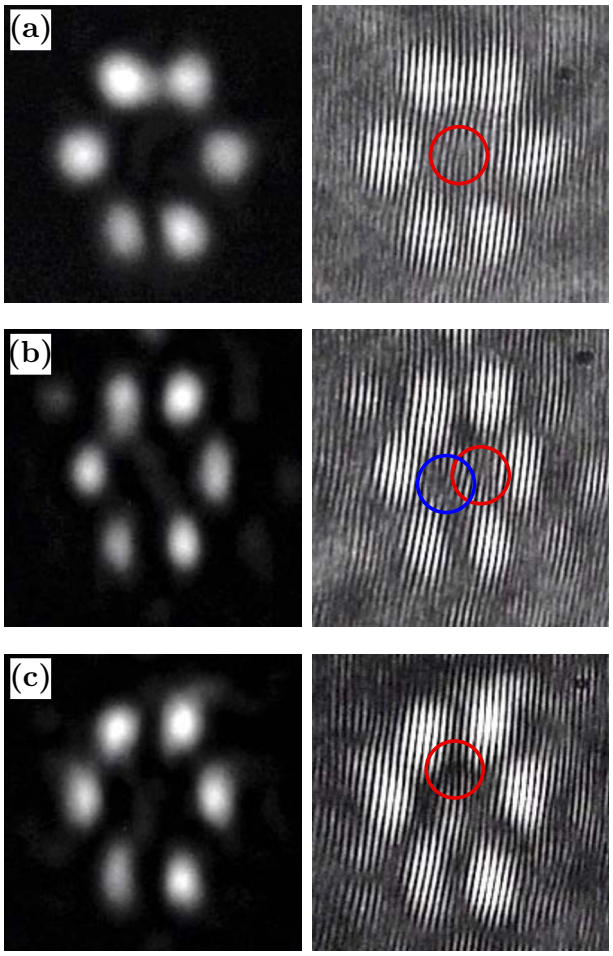

FIG. 10. (Color online) (a) An input single-charge vortex beam in the defocusing regime; (b) the beam profile and phase at the output crystal face for low input intensity; (c) output for high input intensity showing generation of a stable single-charge vortex.

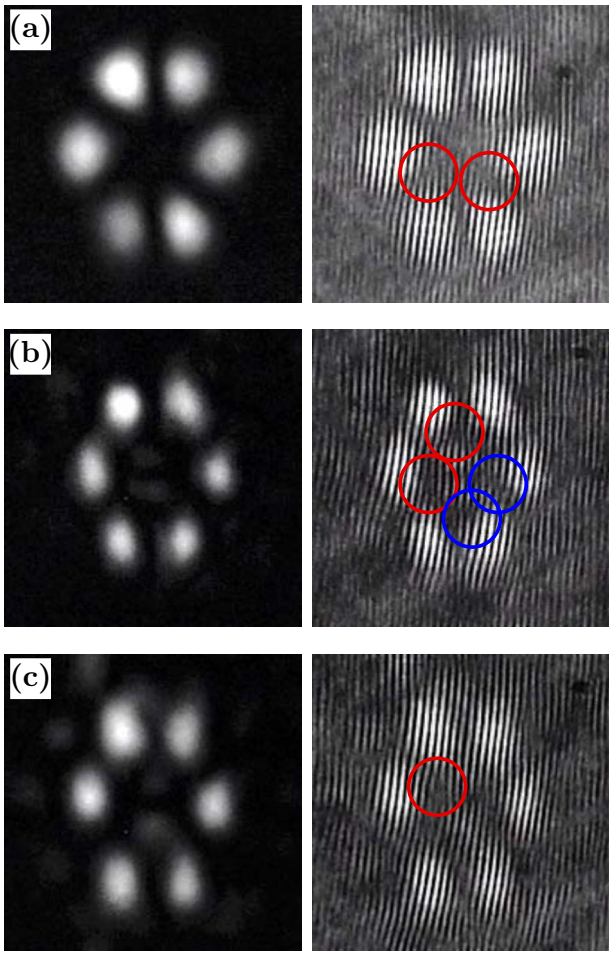

FIG. 11. (Color online) (a) An input double-charge vortex beam in the defocusing regime; (b) the beam profile and phase at the output crystal face for low input intensity; (c) output for high input intensity showing instability of the double-charge vortex.

ers, low power ($I_{\text{probe}} \approx 30$ nW) and high power ($I_{\text{probe}} \approx 160$ nW). Output intensity and phase are then recorded on the beam exit of the crystal.

First, we consider the single-charge vortex input shown in Fig. 10(a). In a good agreement with our numerical simulations, we see only very weak diffraction in the low-power (linear) regime [see Fig. 10(b)]. More importantly, the single-charge vortex phase breaks up, and we observe the emergence of other vortices, indicating that the input beam profile is not stable at low powers. In contrast, at high powers we find that both the intensity and phase profile are well preserved [see Fig. 10(c)], in strong contrast to the observations in the self-focusing nonlinearity case.

In the case of a double-charge vortex input [see Fig. 11(a)], we observe a diffraction pattern similar to that in the single-charge case at low input powers [Fig. 11(b)]. At high input powers, the output shows some diffraction but, more importantly, the vortex phase is again no longer preserved as we are able to identify only a single vortex singularity. This is again in strong contrast to the self-focusing case.

We would like to stress again here that while the stability of the single- and double-charge vortices has been swapped in the defocusing case, with the former now stable, the appearance of the instability is somewhat different between the self-focusing and self-defocusing cases. In the former case, we observed strong intensity modulations which made it clear that the single-charge vortex is unstable. In the defocusing case, the instability development appears to be weaker and to be more evident in the phase than in the intensity. However, we can conclude that the stability properties of the vortices in the defocusing case are inverse to those in the focusing case, as illustrated theoretically above (see also Ref [14].).

VI. CONCLUSIONS

We have demonstrated experimentally the generation of stable double-charge vortex solitons in a hexagonal photonic lattice created optically in a self-focusing photorefractive crystal. We have observed that single-charge vortices are unstable in the same regime and that this main stability property is reversed in the case of defocusing nonlinearity (leading to honeycomb lattices), with the single-charge vortex

appearing to be stable while the double-charge vortex exhibiting a weak instability. It has been shown that these results may be captured numerically in the framework of the full anisotropic model of nonlinear light propagation in photorefractive optical lattices. Furthermore, we have examined the importance of balancing the nonlinearity anisotropy by stretching the lattice and demonstrated analytically, through a discrete model, that beyond a critical imbalance no stable double-charge vortices exist.

ACKNOWLEDGMENTS

The authors acknowledge support from the Australian Research Council, NSF-DMS (through Grants No. NSF-DMS-0349023 and No. NSF-DMS-0806762), and the Alexander von Humboldt Foundation. B.T. thanks Nonlinear Physics Center for warm hospitality and acknowledges financial support from the German Academic Exchange Service (DAAD).

[1] A. S. Desyatnikov, Yu. S. Kivshar, and L. Torner, in *Progress in Optics*, edited by E. Wolf (Elsevier, Amsterdam, 2005), Vol. 47, pp. 291–391.

[2] D. N. Neshev, T. J. Alexander, E. A. Ostrovskaya, Yu. S. Kivshar, H. Martin, I. Makasyuk, and Z. Chen, Phys. Rev. Lett. **92**, 123903 (2004).

[3] J. W. Fleischer, G. Bartal, O. Cohen, O. Manela, M. Segev, J. Hudock, and D. N. Christodoulides, Phys. Rev. Lett. **92**, 123904 (2004).

[4] G. Bartal, O. Manela, O. Cohen, J. W. Fleischer, and M. Segev, Phys. Rev. Lett. **95**, 053904 (2005).

[5] A. Ferrando, M. Zacares, M. A. Garcia-March, J. A. Monsoriu, and P. F. de Cordoba, Phys. Rev. Lett. **95**, 123901 (2005).

[6] T. J. Alexander, A. A. Sukhorukov, and Yu. S. Kivshar, Phys. Rev. Lett. **93**, 063901 (2004).

[7] A. Bezryadina, D. N. Neshev, A. S. Desyatnikov, J. Young, Z. G. Chen, and Yu. S. Kivshar, Opt. Express **14**, 8317 (2006); see also, A. Bezryadina, E. Eugenieva, and Z. Chen, Opt. Lett. **31**, 2456 (2006).

[8] P. G. Kevrekidis, B. A. Malomed, and Yu. B. Gaididei, Phys. Rev. E **66**, 016609 (2002).

[9] V. Koukouloyannis and R. S. MacKay, J. Phys. A **38**, 1021 (2005).

[10] O. Peleg, G. Bartal, B. Freedman, O. Manela, M. Segev, and D. N. Christodoulides, Phys. Rev. Lett. **98**, 103901 (2007).

[11] C. R. Rosberg, D. N. Neshev, A. A. Sukhorukov, W. Krolikowski, and Yu. S. Kivshar, Opt. Lett. **32**, 397 (2007).

[12] T. J. Alexander, A. S. Desyatnikov, and Yu. S. Kivshar, Opt. Lett. **32**, 1293 (2007).

[13] B. Terhalle, T. Richter, A. S. Desyatnikov, D. N. Neshev, W. Krolikowski, F. Kaiser, C. Denz, and Y. S. Kivshar, Phys. Rev. Lett. **101**, 013903 (2008).

[14] K. J. H. Law, P. G. Kevrekidis, T. J. Alexander, W. Krolikowski, and Y. S. Kivshar, Phys. Rev. A **79**, 025801 (2009).

[15] Y. V. Kartashov, A. Ferrando, A. A. Egorov, and L. Torner, Phys. Rev. Lett. **95**, 123902 (2005).

[16] B. Terhalle, A. S. Desyatnikov, C. Bersch, D. Träger, L. Tang, J. Imbrock, Yu. S. Kivshar, and C. Denz, Appl. Phys. B: Lasers Opt. **86**, 399 (2007).

[17] N. K. Efremidis, S. Sears, D. N. Christodoulides, J. W. Fleischer, and M. Segev, Phys. Rev. E **66**, 046602 (2002).

[18] R. Fischer, D. Träger, D. N. Neshev, A. A. Sukhorukov, W. Krolikowski, C. Denz, and Yu. S. Kivshar, Phys. Rev. Lett. **96**, 023905 (2006).

[19] D. Träger, R. Fischer, D. N. Neshev, A. A. Sukhorukov, C. Denz, W. Krolikowski, and Yu. S. Kivshar, Opt. Express **14**, 1913 (2006).

[20] A. Ya. Bekshaev, M. S. Soskin, and M. V. Vasnetsov, Opt. Commun. **241**, 237 (2004).

[21] A. A. Zozulya, D. Z. Anderson, A. V. Mamaev, and M. Saffman, Phys. Rev. A **57**, 522 (1998).

[22] D. E. Pelinovsky, P. G. Kevrekidis, and D. J. Frantzeskakis, Physica D **212**, 1 (2005); **212**, 20 (2005); see also M. Lukas, D. E. Pelinovsky, and P. G. Kevrekidis, *ibid.* **237**, 339 (2008).

[23] D. N. Christodoulides and R. I. Joseph, Opt. Lett. **13**, 794 (1988); Yu. S. Kivshar and M. Peyrard, Phys. Rev. A **46**, 3198 (1992).